Supporting Information

Defect Engineered MoS_2 Nanostructures for ROS Generation in Dark: Anti-Pollutant and Anti-Fungal Performances

Parbati Basu[1], Jayita Chakraborty[2], Nirmal Ganguli[2], Khushi Mukherjee[3], Krishnendu Acharya[3], Biswarup Satpati[4], Sudipta Khamrui[5], Suman Mandal[5], Debmalya Banerjee[5], Dipak Goswami[5], Padinharu M.G. Nambissan[6], Kuntal Chatterjee[1*]

[1]*Department of Physics, Vidyasagar University, Midnapore – 721102, India*
[2] *Department of Physics, IISER Bhopal, Bhauri, Bhopal-462066, India*
[3]*Molecular And Applied Mycology And Plant Pathology Laboratory, Department of Botany, University of Calcutta, Kolkata-700019, India*
[4]*Surface Physics and Materials Science Division, Saha Institute of Nuclear Physics, Bidhannagar, Kolkata- 700064, India*
[5] *Department of Physics, IIT Kharagpur, Kharagpur-721302, India*
[6]*Applied Nuclear Physics Division, Saha Institute of Nuclear Physics, Bidhannagar, Kolkata-700064, India*

** Corresponding author: E mail: kuntal@mail.vidyasagar.ac.in*

Table of contents

S1 Methods:

S1.1 Characterisation:

X-ray diffraction patterns for the powdered samples were obtained from Rigaku Mini-Flex X-ray diffractometer using Cu Kα radiation of wavelength 1.54178Å. The data were recorded in the 2Θ range 3-80◦ with a step width of 0.02◦.Morphological analysis was done by MERLIN(Carl Zeiss) scanning electron microscope and FEI made Tecnei S-twin transmission electron microscope with an accelerating voltage of 200 KV and resolution of 0.24 nm. Raman spectra was recorded on a Model T64000 spectrometer of Jobin Yvon Horiba make equipped with an Argon-Krypton mixed gas laser of Model 2018 RM from Make Spectra Physics as the excitation source. All spectra were recorded at room temperature with an excitation of 488 nm. X-ray photoelectron spectroscopy was done on ULVAC-PHI5000 Versa Probe II Al K_α radiation source of photon energy 1486.6 eV.

S1.2 Dye Removal Studies:

All the dye removal experiments were carried out in dark and at room temperature. Initially, 5mg each of M6, M10 and M*10 were added separately to 25 ml solutions of Methylene blue of different concentrations, ranging between 20 ppm to 160 ppm. The concentration of the dye solutions were increased in steps of 20 ppm. The dispersions were stirred at 240 *rpm* on magnetic stirrer in dark for 24 hours to ensure establishment of complete adsorption-desorption equilibrium. Later, the supernatants were collected, centrifuged and the equilibrium concentrations of Methylene blue were determined at 665 nm using the Shimadzu UV-1700 spectrophotometer. The calibration curves for each dye at the respective wavelength corresponding to maximum absorbance were done as a function of dye concentration, prior to the experiments. The concentration of residual dye was determined using these calibration curves. Similarly, 5 mg of M6 were added to different concentrations of Rhodamine b, Malachite green and Congo Red, ranging between 20 ppm to 100 ppm and exactly same procedure as stated earlier was done. For the kinetic studies 5 mg of each of M6, M10 and M*10 were added separately to 60 ml solutions of 10 ppm Methylene blue and were kept stirring on a magnetic stirrer at 300 *rpm.* At regular intervals, aliquots of 4 ml were withdrawn, centrifuged and the residual dye concentration in it was estimated according to procedure mentioned above. The experiments were repeated four times to ensure the reproducibility of the results.

S1.3 Hydrogen Peroxide Estimation:

Hydrogen peroxide generated from aqueous suspensions of the prepared MoS_2 samples were quantitatively estimated by standard $KMnO_4$ titration method.[1] At regular intervals, 20 ml aliquots of the MoS_2 suspensions(0.38gm/l), kept under constant stirring in dark and at room temperature were filtered through a membrane filter. To these aliquots, requisite amounts of

0.002 M $KMnO_4$ solution and 2 ml of diluted H_2SO_4 were added and the amounts of H_2O_2 formed were estimated by standard titration using a known amount of H_2O_2.

S1.4 Detection of Hydroxyl ($^{\bullet}OH$) radical generation:

The generation of the reactive oxygen species $^{\bullet}OH$ was detected by fluorescence spectroscopy using Terephthalic acid(TA) as the probe. TA which is otherwise non fluorescent, forms 2-Hydroxyl Terephthalic acid complex with $^{\bullet}OH$, which gives fluorescence and its intensity is a direct measure of radical concentration.[2] In a typical process, 5 mM of TA was added to aqueous suspensions of the prepared MoS_2 (1 gm/l) kept under constant stirring at ambient temperature and in dark. At regular intervals, 4 ml aliquots were withdrawn and centrifuged at 5000 rpm and the intensity of emission at 425 nm for an excitation wavelength of 312 nm was monitored as a direct measure of hydroxyl radical generation. The LS 55 fluorescence spectrometer from Perkin Elmer was used for recording the intensity of emission at 425nm for an excitation wavelength of 312 nm.

S1.5 Superoxide detection:

The spectrophotometric reduction of Nitro blue tetrazolium (NBT) was used to qualitatively assess the generation of superoxide anion radical ($^{\bullet}O_2^-$) by MoS_2 in dark. A stock solution of strength 5 mM of NBT was prepared. In a typical procedure, to 20 ml of the 5mM NBT solution, 5mg of the respective samples were added and were constantly stirred in dark. At regular intervals, 4 ml aliquots were withdrawn and centrifuged at 5000 rpm. The supernatant was collected and the absorbance maxima of NBT at 259 nm was monitored using Shimadzu UV-1700 spectrophotometer to evaluate the formation of $^{\bullet}O_2^-$ which converts NBT to monoformazon and diformazon[3].

S1.6 Antifungal Studies:

S1.6.1Maintenance of fungal culture:

Fungal pathogen *Alternaria alternata* was sub-cultured in Potato Dextrose Agar (PDA) and incubated at 28˚C for 7 days. The mature culture was stored at 4˚C. The fungus was freshly grown prior to every experiment.

S1.6.2 Fungitoxicity assay:

Different aliquots of nanoparticles were incorporated into the PDA plated to achieve the desired nanoparticle concentrations. The fungal mycelia of 5mm diameter were inoculated into the nanoparticle containing PDA plates and incubated at 28˚C temperature. Radial growth of the fungal colonies was measured after 7 days. Nanoparticle induced fungal growth inhibition was

calculated with reference to the control experiment (devoid of NP). The experiments were carried out both in dark and ambient light.[4]

S1.6.3 Scanning Electron Microscopy (SEM):

Nanoparticle induced deformities in fungal mycelia were studied under Electron Microscope (ZEISS EVO 18 Special Edition) and compared with the untreated one as the reference.●

S1.7 Electron Paramagnetic Resonance study:

The X-band EPR signals were recorded at room temperature on ELEXSYS E580 pulsed electron paramagnetic resonance spectrometer from Bruker. The microwave operating frequency was maintained between 9.6508 Ghz to 99.6594Ghz(X-band) and the microwave power was fixed at 15mW.

S1.8 Positron Annihilation Spectroscopic Studies:

For the positron annihilation spectroscopy (PAS) experiments, a ^{22}Na ($\sim$10 μCi) radioactive isotope was embedded at the geometrical centre of the volume of the powdered samples taken in a glass tube of approximately 10 mm diameter. The adequate amount of the powdered samples embedded the ^{22}Na source in such a way that positrons did not penetrate to the walls of the glass tube but are completely annihilated within the sample only. Earlier, the positron source was prepared by the deposition of ^{22}NaCl dissolved in dilute hydrochloric acid on a thin Ni foil (~ 2 mg.cm^{-2}) and dried and the extended portion of the foil was folded along a line away from the source deposited area in order to cover and protect the source deposition from contamination by the used sample. The Ni foil had been annealed at 1050^{o}C for 2 hours in adequate vacuum (~ 10^{-6} mbar) prior to the source deposition. During the experimental procedure and data acquisition, the glass tube containing the powdered sample and the source was continuously evacuated to remove any air or absorbed gases within the sample column, thereby allowing the particles to settle down due to their own weight. Thus, throughout the entire course of experiments, the glass tube containing the source-sample assembly was maintained in clean and moisture free conditions.

In the case of positron lifetime measurements, the gamma rays were detected using BaF_2 scintillators coupled with XP2020Q photomultiplier tubes. The positron lifetime measurements were carried out using a slow-fast gamma-gamma positron lifetime spectrometer, which had a time resolution (full width at half maximum of ^{60}Co gamma rays coincidence spectrum) of 180 ps under the selected ^{22}Na experimental energy settings. Typically, about 10^6 counts were recorded under each spectrum and the recorded data were analysed using the PALSfit program.[5]

In the coincidence Doppler broadening spectroscopy (CDBS) experiments, the gamma ray events at energies E_1 and E_2 (i.e., 511+/- ΔE respectively) were recorded using two high pure

germanium (HPGe) detectors with energy resolutions of 1.27 keV and 1.33 keV respectively at the annihilation gamma ray energy of 511 keV. A two-parameter spectrum was generated with $E_1 + E_2$ and $E_1 - E_2$ as coplanar axes and counts distributed in the third axis. The projection of the segment under $E_1 + E_2 = 1022 \pm 1.45$ keV onto the axis parallel to the energy difference $E_1 - E_2$ axis was analysed by the quotient method to obtain the ratio curves for the samples studied.[6] The CDBS data acquisition, storage and analysis were done using the LAMPS software, developed by the Pelletron division of Tata Institute of Fundamental Research, Mumbai.

S1.9 DFT calculations:

The atomic positions are optimized to minimize the Hellman–Feynman force on each atom with a tolerance value of 0.01 eV/Å.

We have considered the possibility of doping nitrogen at Mo as well as S site of MoS2 in 1T and 2H structural phases. The formation energy of such doping may be defined as[7-8]

$$FE = E\left[\mathrm{Mo}_{k-i}\mathrm{S}_{2k-j}\mathrm{N}_{i+j}\right] - E\left[\mathrm{Mo}_{k}\mathrm{S}_{2k}\right] + \sum_{x} n_x \mu_x \quad \text{.....(i)}$$

where i number of Mo atoms and j number of S atoms are considered to have been replaced by $(i+j)$ number of N-atoms [i, j are integers; $0 \leq i < k$; $0 \leq j < 2k$]. x is the type of atom added to or removed from the pure Mo_kS_{2k} structure in the process of doping. For example, the process of doping one N atom in Mo_kS_{2k} structure replacing one S atom to form $Mo_kS_{2k-1}N$ can be represented by $n_N = +1$ and $n_S = -1$. μ_x is the chemical potential for adding or removing atom x. The chemical potential of N is the energy per atom in its molecular form (gas phase). The chemical potential for S and Mo can vary over a range allowed by the relation $E(\mathrm{MoS_2}) = \mu_{\mathrm{Mo}} + 2\mu_{\mathrm{S}}$, where the maximum limit corresponds to the energy per atom in the standard elemental structure. In the present work, the maximum limit of the chemical potential of sulphur (S-rich limit) was obtained from the energy per S atom in the α phase [9] that consists of S8 puckered rings packed in an orthorhombic lattice

S2 Results and discussions:

S2.1 X-ray diffraction studies:

The atomic plane spacing in the MoS_2 nanostructures can be calculated from the X-ray diffraction patterns using the Bragg equation:

$$2d \sin\theta = n\lambda \quad \text{.....(ii)}$$

where d is the atomic plane spacing, θ is the Bragg scattering angle and λ is the wavelength of the incident X-ray. In addition to calculated d_{002} which show larger interlayer spacing for (002) planes, the d_{100} also showed an increasing trend from M6 to M*10.

Using the calculated d_{100} and d_{002} values we can calculate the lattice constants *a* and *c* by

$$1/d^2 = \frac{4}{3}\frac{(h^2 + hk + k^2)}{a^2} + \frac{l^2}{c^2} \quad \text{.....(iii)}$$

for hexagonal lattice , and

$$1/d^2 = \frac{(h^2 + k^2 + l^2)(\sin\theta)^2 + \{(\cos\alpha)^2 - \cos\alpha\}}{a^2\{1 - 3(\cos\alpha)^2 + 2(\cos\alpha)^3\}} \quad \text{.....(iv)}$$

for rhombohedral lattices.

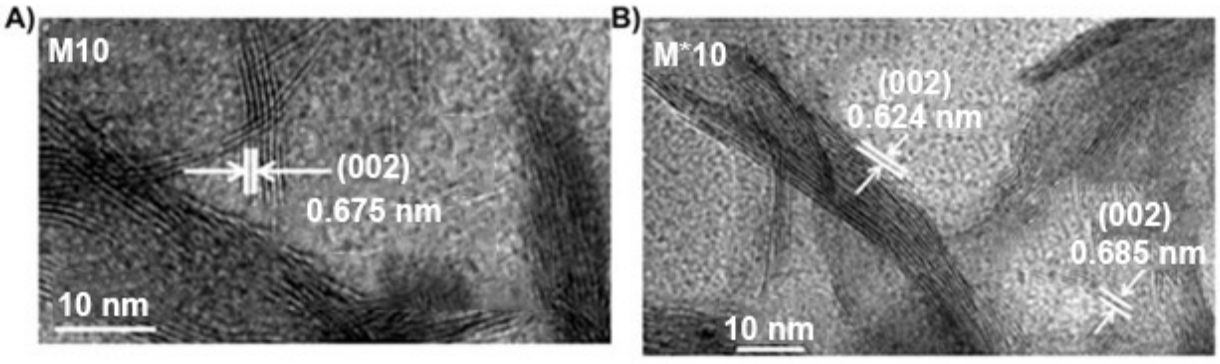

Figure S1: HRTEM images of A) M10 B) M*10

S2.2 X-ray photoelectron spectroscopy studies:

S2.2.1 Deconvolution of high resolution XPS spectra:

The deconvolution of the multi-component XPS spectra was done using mixed Gaussian Lorentzian product function along with a Shirley background correction using CASAXPS. The lower binding energy component at about 530.5-531 *eV* in the O 1s spectra is due to the unreacted MoO_3 in the sample.[10-12] The components near 531.5 eV corresponds to oxygen in -OH groups[13-14] while those at 532.55 *eV* and 533.36 *eV* adsorbed oxygen from atmosphere and physiosorbed or chemisorbed water at the surface[14-16].

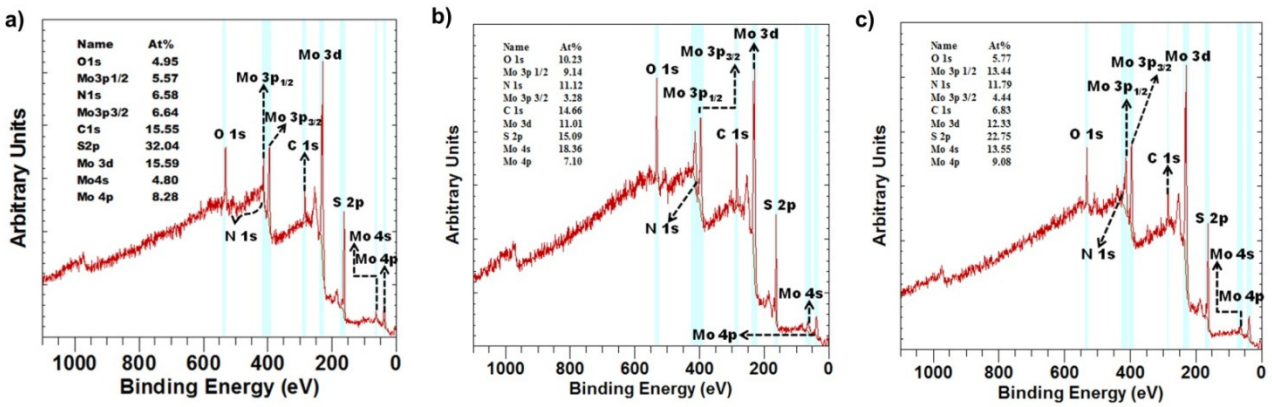

Figure S2: XPS survey spectra of a) M6, b) M10 and c) M*10 samples

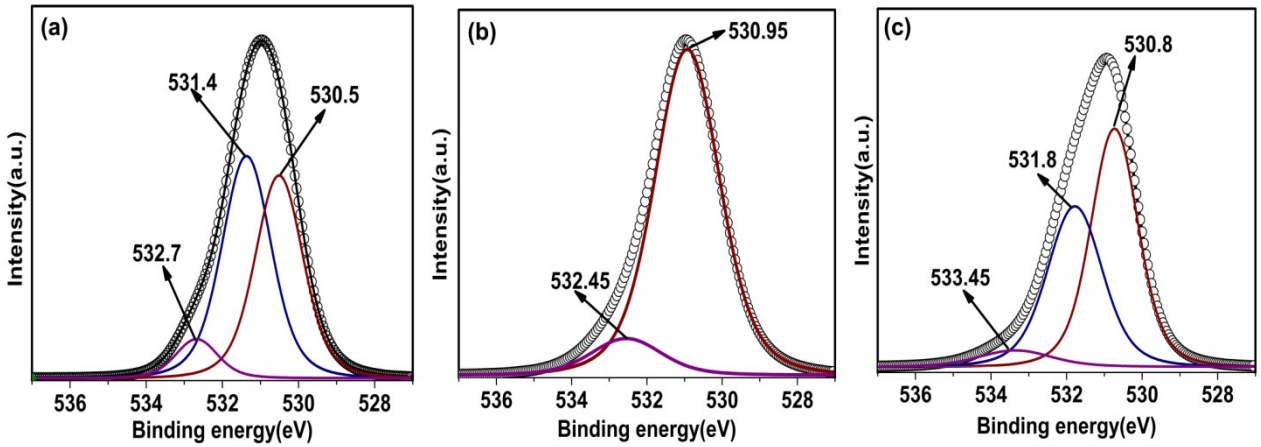

Figure S3: The high resolution XPS spectra from O 1s region of a) M6, b) M10 and c) M*10

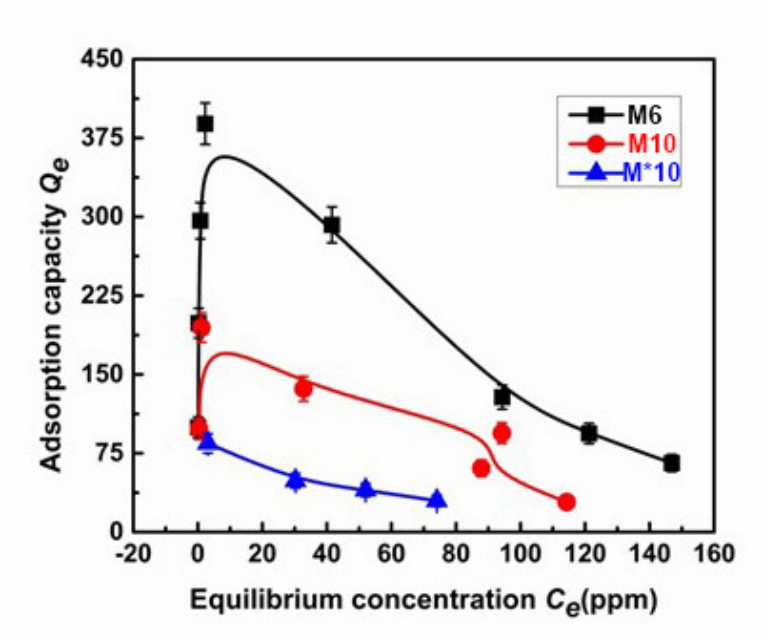

Figure S4: Q_e *vs* C_e plot for the prepared samples.

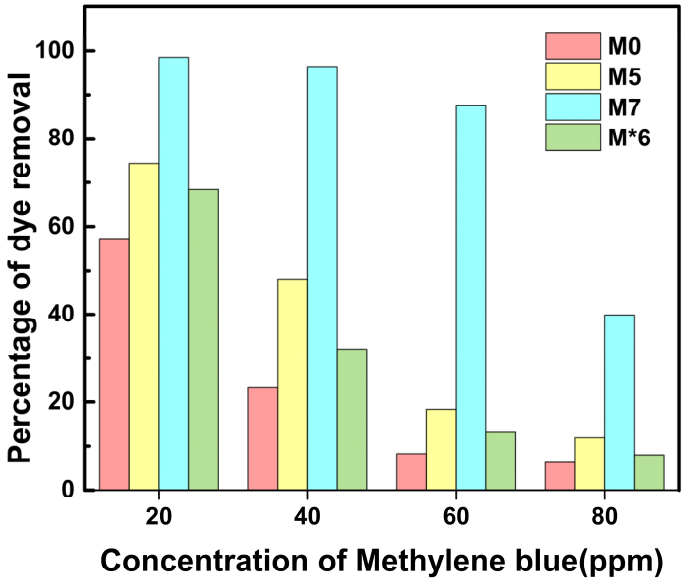

Figure S5: Metheylene blue removal results of M0, M5, M7, M*6 dark

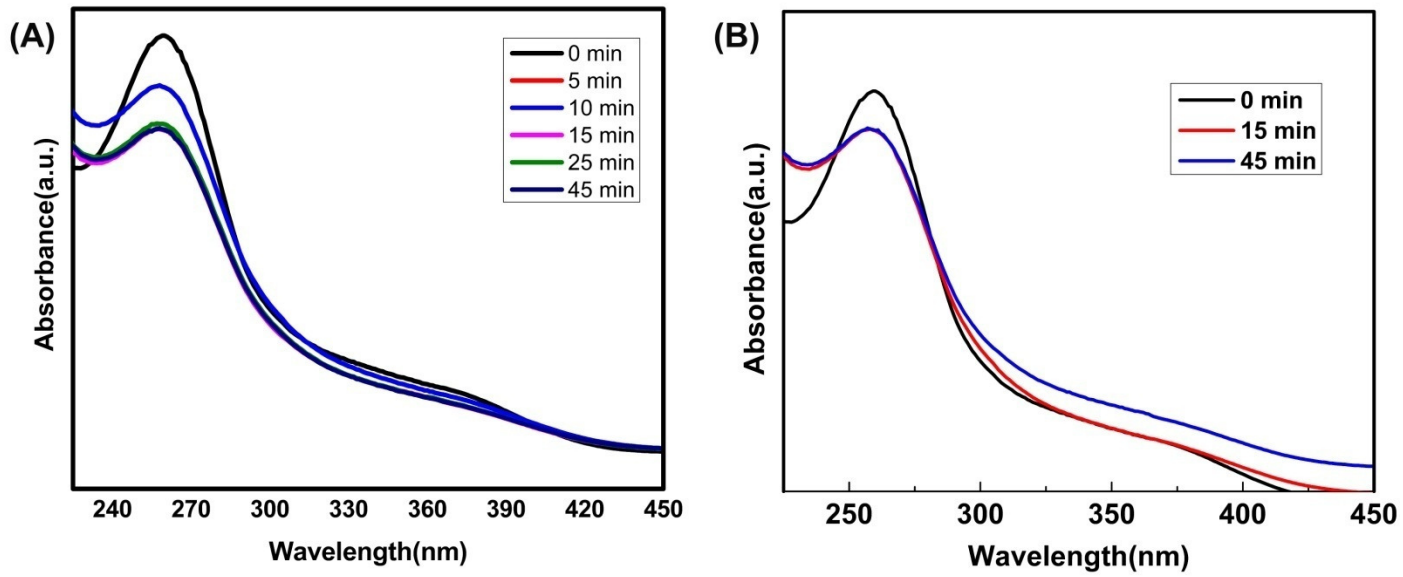

Figure S6: NBT degradation by A) M10, B) M*10

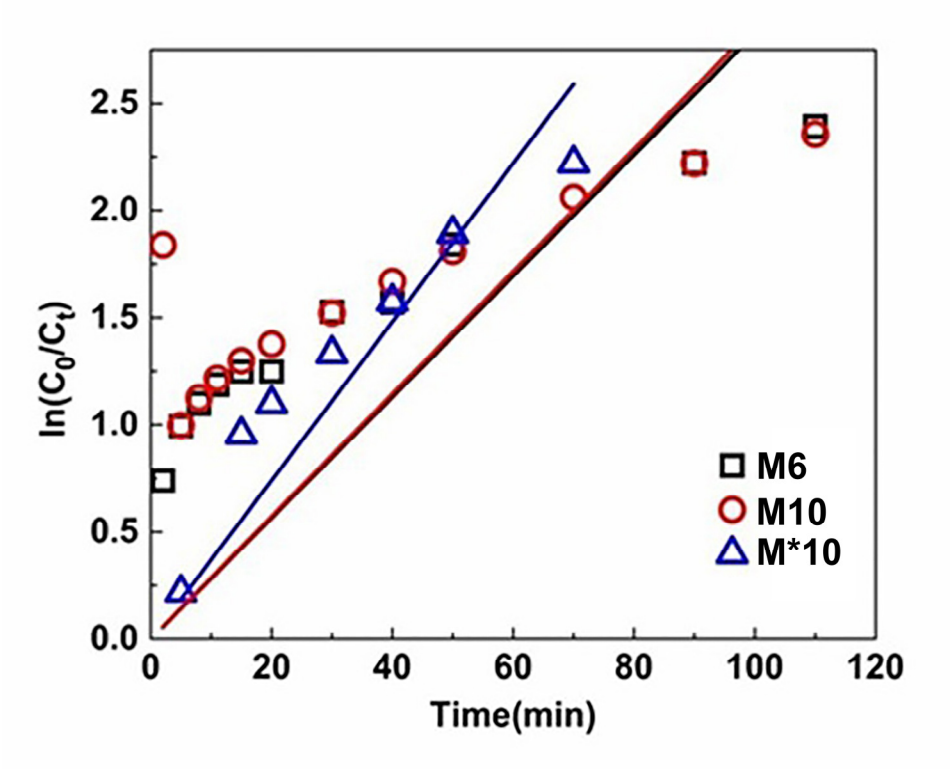

Figure S7: Plots of first order kinetic model

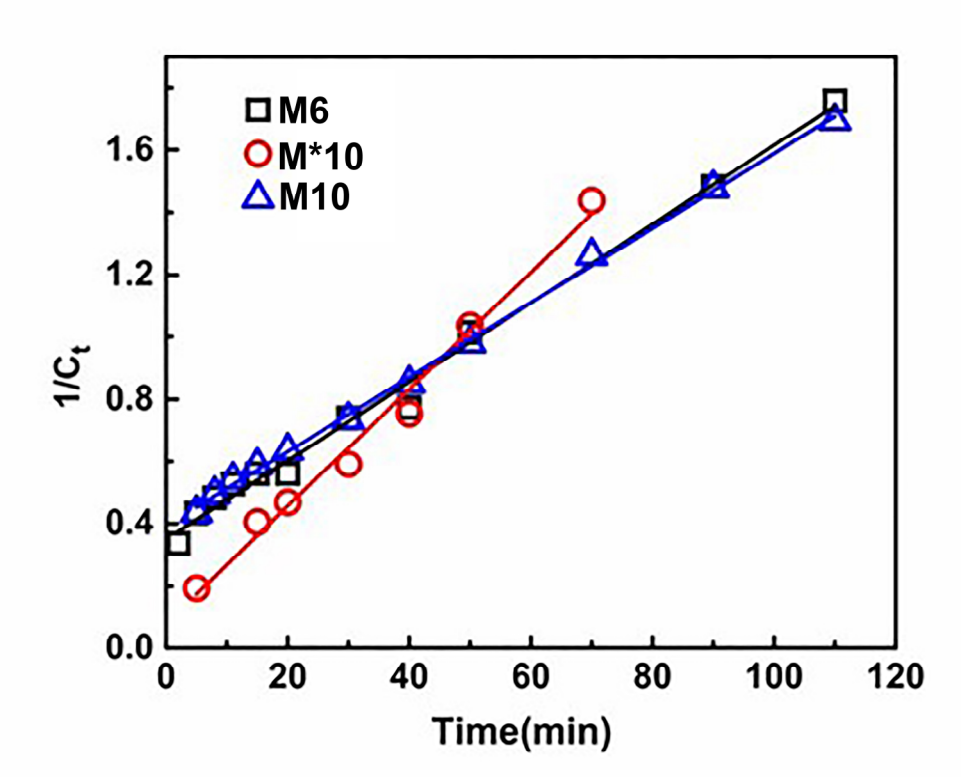

Figure S8: Plots of second order kinetic model

TABLE S1: Fitting results of the kinetic models:

	M6	M10	M*10
First order kinetic model:			
k_1 (ppm/min)	0.0283	0.0286	0.037
R^2	0.776	0.725	0.962
Second order kinetic model:			
k_2(ppm/min)	0.0127	0.0119	0.0188
R^2	0.992	0.998	0.985

TABLE-S2 : Dye removal studies of MoS_2 based nanomaterials. Here MB and RhB stand for Methylene blue and Rhodamine B respectively

Sample	Dyes	Removal capacity	Removal time	Concen-tration of dyes	Sample dosage	Mechanism of removal	Reference
Nitrogen doped MoS_2	MB	97.148-99.55	24 hours	20-80	0.2	ROS generation in dark + Adsorption	This study
N-doped MoS_2	Methyl Orange	89.6	60 min	50	0.4	Adsorption	Lu *et al.*[17]
Flower like MoS_2	RhB	91	90 min	20	1.0	Adsorption	Wang *et al.*[18]
Hiererchical microspheres of MoS_2	MB	92.4	24 hours	120	1.0	Adsorption	Massey *et al.*[19]
ZnO coated MoS_2	RhB	68.3	90 min	-	0.5	Photocatalytic + Adsorption	Tian *et al.*[20]
Polyanaline@ MoS_2	Congo Red	35.46	6 hours	100	0.5	Adsorption	Kumar *et al.* [21]
Fe_3O_4@MoS_2	Congo Red	71.4	120 min	100	1.0	Adsorption	Song *et al.*[22]

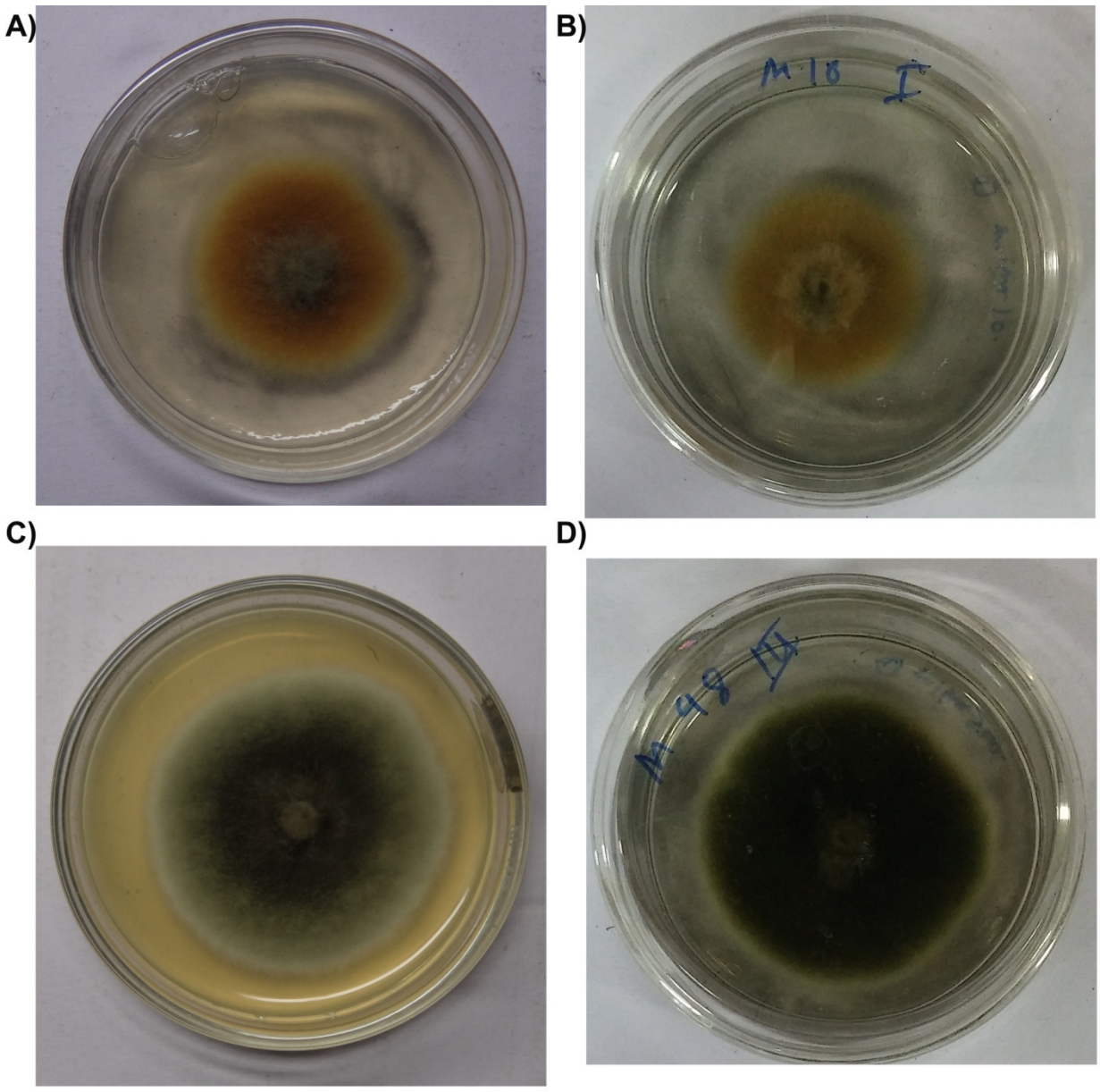

Figure S9: Digital photographs of *Alternaria alternata* colony grown in the presence of M10 A) in dark; B) under visible light exposure; and in presence of M*10 C) in dark; and D) under visible light exposure

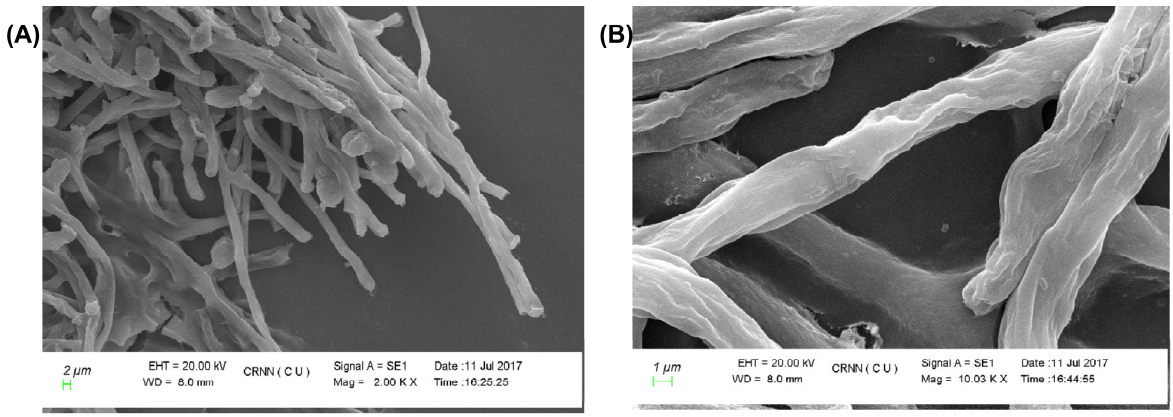

Figure S10: SEM micrographs of *A. alternata* mycelia grown in dark in presence of (A) M10 and (B) M*10

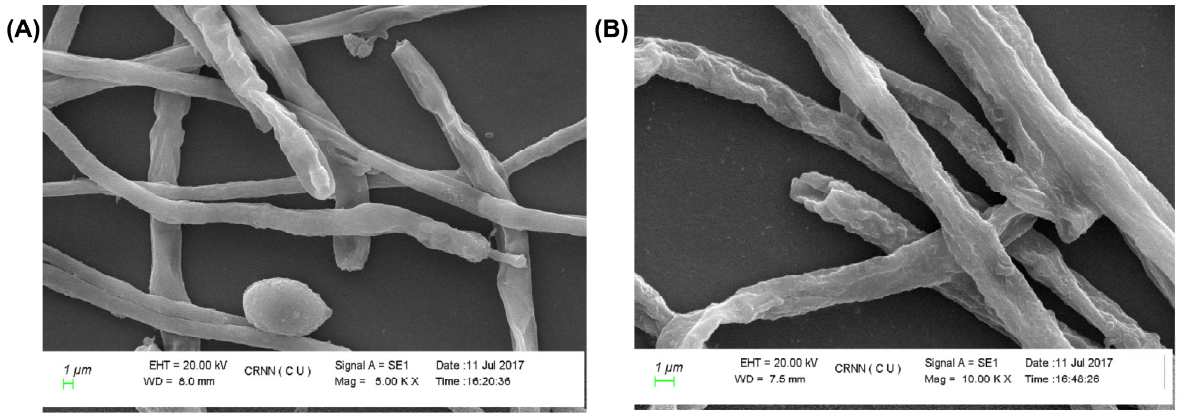

Figure S11: SEM micrographs of *A. alternata* mycelia grown under visible light illumination in presence of (A) M10 and (B) M*10

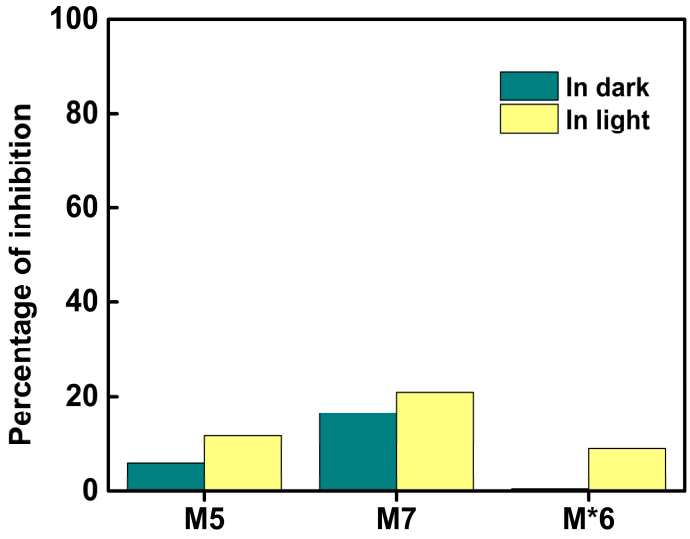

Figure S12: Growth inhibitory effects of M5, M7 and M*6 on A.alternata under dark and visible light exposure

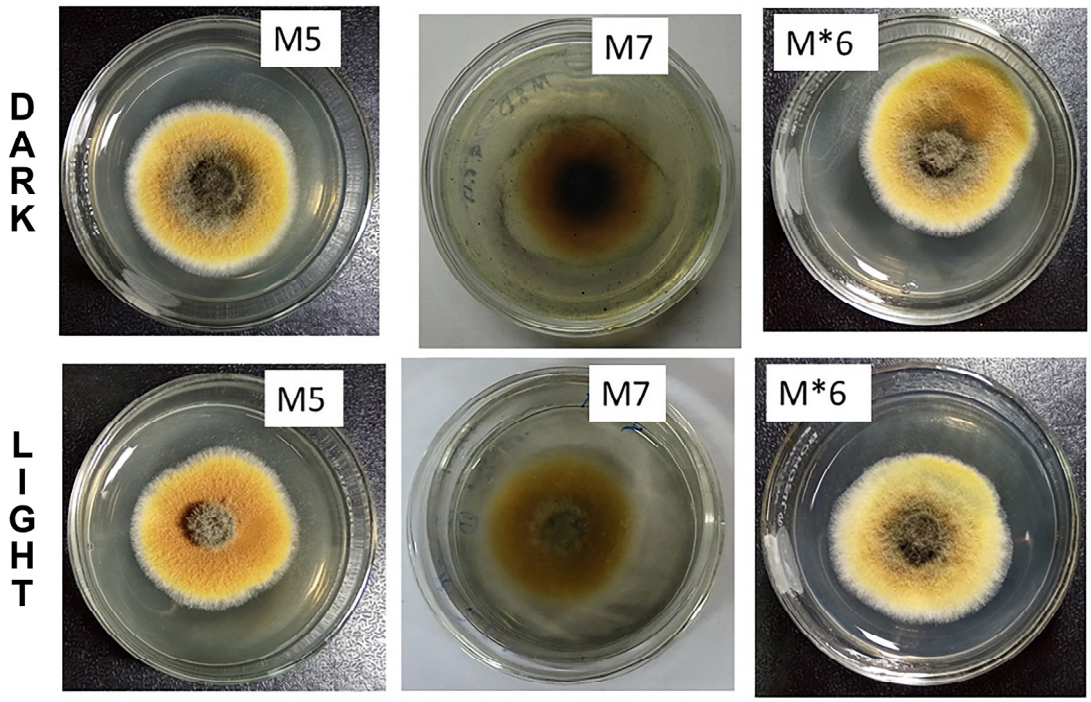

Figure S13: Digital photographs of *Alternaria alternata* colony grown in the presence of M5, M7 and M*10 both in dark and under visible light exposure.

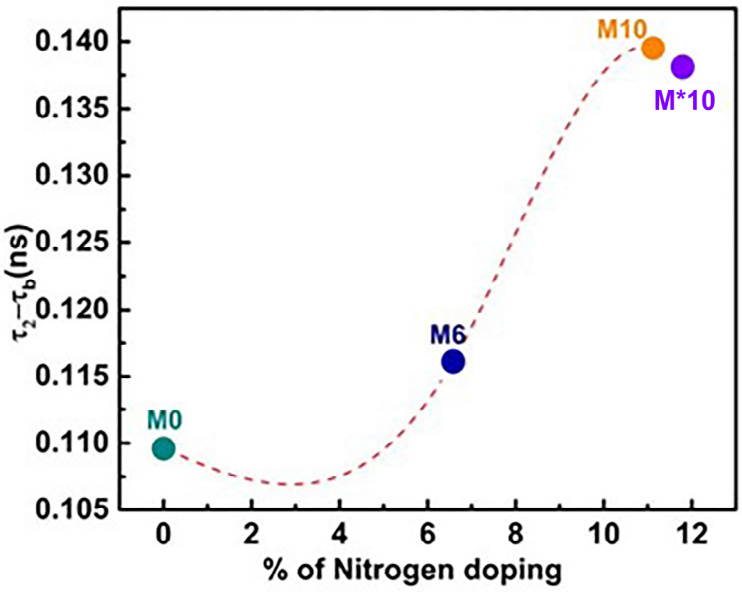

Figure S14: The variation of $\tau_2 - \tau_b$ with nitrogen doping

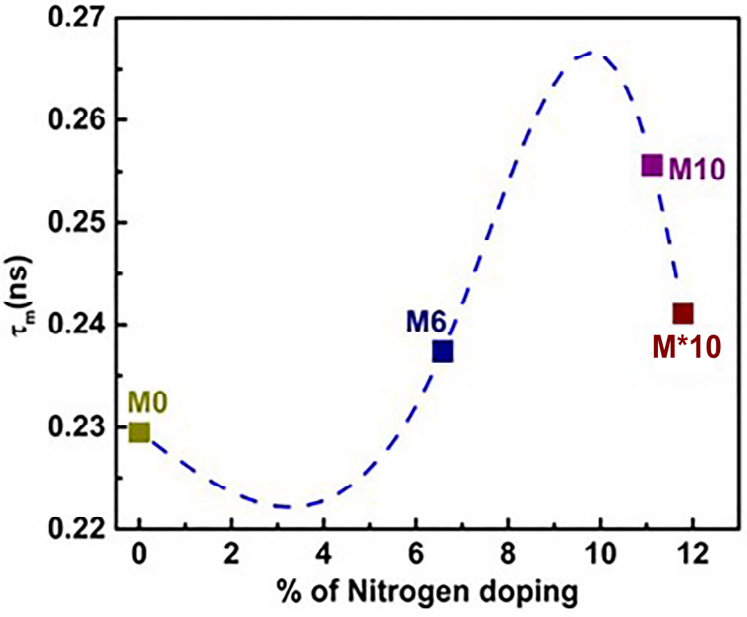

Figure S15: The variation of τ_m with nitrogen doping

REFERENCE

(1) Wolanov, Y.; Prikhodchenko, P. V.; Medvedev, A. G.; Pedahzur, R.; Lev, O. Zinc Dioxide Nanoparticulates: A Hydrogen Peroxide Source at Moderate pH. *Environmental science & technology* 2013, *47* (15), 8769-8774.

(2) Xu, X.; Chen, D.; Yi, Z.; Jiang, M.; Wang, L.; Zhou, Z.; Fan, X.; Wang, Y.; Hui, D. Antimicrobial Mechanism Based on H_2O_2 Generation at Oxygen Vacancies in ZnO Crystals. *Langmuir* 2013, *29* (18), 5573-5580.

(3) Goto, H.; Hanada, Y.; Ohno, T.; Matsumura, M. Quantitative Analysis of Superoxide Ion and Hydrogen Peroxide produced from Molecular Oxygen on Photoirradiated TiO2 Particles. *Journal of Catalysis* 2004, *225* (1), 223-229.

(4) Boxi, S. S.; Mukherjee, K.; Paria, S. Ag Doped Hollow TiO_2 Nanoparticles as an Effective Green Fungicide Against Fusarium solani and Venturia inaequalis Phytopathogens. *Nanotechnology* 2016, *27* (8), 085103.

(5) Olsen, J. V.; Kirkegaard, P.; Pedersen, N. J.; Eldrup, M. PALSfit: A New Program for the Evaluation of Positron Lifetime Spectra. *Physica status solidi C* 2007, *4* (10), 4004-4006.

(6) Asoka-Kumar, P.; Alatalo, M.; Ghosh, V.; Kruseman, A.; Nielsen, B.; Lynn, K. Increased Elemental Specificity of Positron Annihilation Spectra. *Physical review letters* 1996, *77* (10), 2097.

(7) Ganguli, N.; Dasgupta, I.; Sanyal, B. The Making of Ferromagnetic Fe doped ZnO Nanoclusters. *Applied Physics Letters* 2009, *94* (19), 192503.

(8) Ganguli, N.; Dasgupta, I.; Sanyal, B. Electronic Structure and Magnetism of Transition Metal Doped $Zn_{12}O_{12}$ Clusters: Role of Defects. *Journal of Applied Physics* 2010, *108* (12), 123911.

(9) Moore, C. E.; Russell, H. N. Binding Energies for Electrons of Different Types. *Journal of Research of the National Bureau of Standards* 1952, *48* (1), 61.

(10) Zingg, D.; Makovsky, L. E.; Tischer, R.; Brown, F. R.; Hercules, D. M. A Surface Spectroscopic Study of Molybdenum-Alumina Catalysts using X-ray Photoelectron, Ion-Scattering, and Raman Spectroscopies. *The Journal of Physical Chemistry* 1980, *84* (22), 2898-2906.

(11) Nefedov, V.; Firsov, M.; Shaplygin, I. Electronic Structures of $MRhO_2$, MRh_2O_4, $RhMO_4$ and Rh_2MO_6 on the basis of X-ray Spectroscopy and ESCA data. *Journal of Electron Spectroscopy and Related Phenomena* 1982, *26* (1), 65-78.

(12) Patterson, T. A.; Carver, J. C.; Leyden, D. E.; Hercules, D. M. A Surface Study of Cobalt-Molybdena-Alumina Catalysts using X-ray Photoelectron Spectroscopy. *The Journal of Physical Chemistry* 1976, *80* (15), 1700-1708.

(13) Tan, B. J.; Klabunde, K. J.; Sherwood, P. M. XPS Studies of Solvated Metal Atom Dispersed (SMAD) Catalysts. Evidence for Layered Cobalt-Manganese Particles on Alumina and Silica. *Journal of the American Chemical Society* 1991, *113* (3), 855-861.

(14) Dickinson, T.; Povey, A. F.; Sherwood, P. M. Dissolution and Passivation of Nickel. An X-ray Photoelectron Spectroscopic Study. *Journal of the Chemical Society, Faraday Transactions 1: Physical Chemistry in Condensed Phases* 1977, *73*, 327-343.

(15) Zhang, C.; Sunarso, J.; Liu, S. Designing CO_2-Resistant Oxygen-Selective Mixed Ionic–Electronic Conducting Membranes: Guidelines, Recent Advances, and Forward Directions. *Chemical Society Reviews* 2017, *46* (10), 2941-3005.

(16) Knipe, S.; Mycroft, J.; Pratt, A.; Nesbitt, H.; Bancroft, G. X-ray Photoelectron Spectroscopic Study of Water Adsorption on Iron Sulphide Minerals. *Geochimica et Cosmochimica Acta* 1995, *59* (6), 1079-1090.

(17) Lu, H.; Wang, J.; Tian, B.; Huang, X.; Bi, J.; Wang, T.; Hao, H. Application of N-Doped MoS_2 Nanocrystals for Removal of Azo Dyes in Wastewater. *Chemical Engineering & Technology* 2018, *41* (6), 1180-1187.

(18) Wang, X.; Ding, J.; Yao, S.; Wu, X.; Feng, Q.; Wang, Z.; Geng, B. High Supercapacitor and Adsorption Behaviors of Flower-like MoS_2 Nanostructures. *Journal of Materials Chemistry A* 2014, *2* (38), 15958-15963.

(19) Massey, A. T.; Gusain, R.; Kumari, S.; Khatri, O. P. Hierarchical Microspheres of MoS_2 Nanosheets: Efficient and Regenerative Adsorbent for Removal of Water-Soluble Dyes. *Industrial & Engineering Chemistry Research* 2016, *55* (26), 7124-7131.

(20) Tian, Q.; Wu, W.; Yang, S.; Liu, J.; Yao, W.; Ren, F.; Jiang, C. Zinc Oxide Coating Effect for the Dye Removal and Photocatalytic Mechanisms of flower-like MoS_2 Nanoparticles. *Nanoscale research letters* 2017, *12* (1), 221.

(21) Kumar, R.; Ansari, S. A.; Barakat, M.; Aljaafari, A.; Cho, M. H. A Polyaniline@ MoS_2-based Organic–Inorganic Nanohybrid for the Removal of Congo Red: Adsorption Kinetic, Thermodynamic and Isotherm Studies. *New Journal of Chemistry* 2018, *42* (23), 18802-18809.

(22) Song, H. J.; You, S.; Jia, X. H.; Yang, J. MoS_2 Nanosheets Decorated with Magnetic Fe_3O_4 Nanoparticles and Their Ultrafast Adsorption for Wastewater Treatment. *Ceramics International* 2015, *41* (10), 13896-13902.